International Journal of Solids and Structures 46 (2009) 1167–1175

Contents lists available at ScienceDirect

International Journal of Solids and Structures

journal homepage: www.elsevier.com/locate/ijsolstr

Orientation-dependent adhesion strength of a rigid cylinder in non-slipping contact with a transversely isotropic half-space

Haimin Yao [a], Shaohua Chen [b], Pradeep R. Guduru [c], Huajian Gao [c,*]

[a] Department of Materials Science and Engineering, Massachusetts Institute of Technology, 77 Massachusetts Avenue, Cambridge, MA 02139, USA
[b] LNM, Institute of Mechanics, Chinese Academy of Sciences, Beijing 100080, China
[c] Division of Engineering, Brown University, Providence, RI 02912, USA

ARTICLE INFO

Article history:
Received 11 July 2008
Received in revised form 10 October 2008
Available online 1 November 2008

Keywords:
Contact mechanics
Anisotropy
Adhesion strength
Barnett–Lothe tensors

ABSTRACT

Recently, Chen and Gao [Chen, S., Gao, H., 2007. Bio-inspired mechanics of reversible adhesion: orientation-dependent adhesion strength for non-slipping adhesive contact with transversely isotropic elastic materials. J. Mech. Phys. solids 55, 1001–1015] studied the problem of a rigid cylinder in non-slipping adhesive contact with a transversely isotropic solid subjected to an inclined pulling force. An implicit assumption made in their study was that the contact region remains symmetric with respect to the center of the cylinder. This assumption is, however, not self-consistent because the resulting energy release rates at two contact edges, which are supposed to be identical, actually differ from each other. Here we revisit the original problem of Chen and Gao and derive the correct solution by removing this problematic assumption. The corrected solution provides a proper insight into the concept of orientation-dependent adhesion strength in anisotropic elastic solids.

1. Introduction

It has been revealed that the extraordinary ability of geckos to climb on vertical walls and ceilings essentially stems from the van der Waals force (Autumn et al., 2000). To take advantage of the extremely weak intermolecular forces, geckos have developed hundreds of thousands of tiny fibers on their feet. Each fiber, referred to as seta, is split further into hundreds of thinner branches called spatulae. Such hierarchical fibrillar structures have apparently allowed gecko to achieve robust adhesion with solid surfaces irrespective of surface roughness (Arzt et al., 2003; Gao and Yao, 2004). More interestingly, the adhesion force of a single seta was found to be strongly dependent on the pulling direction. Strongest adhesion was measured at a pulling angle of around 30° with respect to the surface (Autumn et al., 2000). Such directional adhesion force can be partly attributed to the asymmetrical geometry of a single seta (Gao et al., 2005). On the other hand, the direction-dependent adhesion strength also turns out to be a generic phenomenon associated with anisotropic elastic solids, as shown by Yao and Gao (2006) for a cracked interface between an anisotropic material and a rigid substrate. Chen and Gao (2007) made the first attempt to develop a real contact model for this phenomenon by considering a rigid cylinder in contact with a transversely isotropic elastic solid subjected to an inclined pulling force. As expected, the adhesion force was found to be dependent on the pulling angle. However, an implicit assumption made in the study of Chen and Gao (2007) was that the contact region remains symmetric with respect to the center of the cylinder. It was not realized until recently that this assumption was not self-consistent because the resulting energy release rates at the two contact edges differed from each other. The purpose of this paper is to revisit the original problem of Chen and Gao (2007) and to derive the correct solution without an assumption on the symmetry of the contact region.

2. Barnett–Lothe tensors

Before proceeding to discuss adhesive contact associated with transversely isotropic materials, we briefly introduce the *Barnett–Lothe* tensors (e.g., Ting, 1996), which will be frequently used in the discussions later. For simplicity, here we just list the expressions of the Barnett–Lothe tensors for a transversely isotropic solid (plane strain). Readers are referred to Ting (1996), Dongye and Ting (1989) and Hwu (1993) for more details.

For a transversely isotropic solid, the elastic property can be fully described by five independent constants, which usually consists of the Young's modulus and Poisson ratio in the isotropic plane (E_1 and ν_1), as well as the Young's modulus, Poisson ratio and shear modulus associated with the out-of-plane direction (E_2, ν_2 and G_{12}). The Barnett–Lothe tensors $\mathbf{S}_0$ and $\mathbf{L}_0$ for a transversely isotropic material can be expressed in terms of these five elastic constants as (Hwu, 1993).

* Corresponding author. Tel.: +1 401 863 2626; fax: +1 401 863 9052.
E-mail address: Huajian_Gao@brown.edu (H. Gao).

0020-7683/$ - see front matter © 2008 Elsevier Ltd. All rights reserved.
doi:10.1016/j.ijsolstr.2008.10.011

$$\mathbf{S}_0 = \begin{bmatrix} 0 & s_{12} \\ s_{21} & 0 \end{bmatrix}, \quad \mathbf{L}_0 = \begin{bmatrix} L_{11} & 0 \\ 0 & L_{22} \end{bmatrix}, \tag{1}$$

where

$$s_{12} = -\alpha_2\gamma_1\chi_1, \quad s_{21} = \alpha_1\gamma_2\chi_1, \quad L_{11} = \alpha_1\gamma_1 E_1, \quad L_{22} = \alpha_2\gamma_2 E_2, \tag{2}$$

with

$$\gamma_1 = (E_1/G_{12} + 2\chi_1\sqrt{E_1/E_2})^{-1/2}, \quad \gamma_2 = (E_2/G_{12} + 2\chi_1\sqrt{E_2/E_1})^{-1/2}$$

$$\alpha_1 = (1-\nu_1^2)^{-1/2}, \quad \alpha_2 = \left(1 - \frac{\nu_2^2 E_1}{E_2}\right)^{-1/2},$$

$$\chi_1 = \sqrt{(1-\nu_1^2)\left(1 - \frac{\nu_2^2 E_1}{E_2}\right)} - (1+\nu_1)\nu_2\sqrt{\frac{E_1}{E_2}}.$$

Clearly, one can see that

$$\frac{L_{22}}{L_{11}} = \frac{\alpha_2}{\alpha_1}\sqrt{\frac{E_2}{E_1}}. \tag{3}$$

In general, α_1 and α_2 are constants close to unity. Therefore, Eq. (3) implies that L_{22}/L_{11} represents the degree of elastic anisotropy of the material. For isotropic materials, we have $L_{22}/L_{11} = 1$; nevertheless, $L_{22}/L_{11} = 1$ does not necessarily leads to isotropy. In this paper, we name solids with $L_{22}/L_{11} = 1$ as "quasi-isotropic" materials.

It should be emphasized that the matrix expressions of the Barnett–Lothe tensors for anisotropic materials depend on the coordinate system they refer to. The above expressions hold for a set of Cartesian coordinates with the 2-axis parallel to the symmetric axis of the transversely isotropic material. Proper transformation has to be made in order to get the expressions in a different coordinate system.

3. Theoretical model

Consider a rigid cylinder of radius R in non-slipping adhesive contact with a transversely isotropic half-space, as shown in Fig. 1. The contact sizes on both sides of the apex are denoted by a and b, respectively. Generally, a is not necessarily equal to b. This is the major difference of the present model from the previous work by Chen and Gao (2007). The symmetric axis of the transversely isotropic material is inclined at angle θ with respect to the normal of the surface. A pulling force F is applied on the rigid cylinder at an angle ϕ from the y-axis. For simplicity, we assume that F is applied in such a way that no net bending moment is produced. As a consequence, the rigid cylinder just experiences translation. Note that the actual location of the applied force is not fixed and may depend on the magnitude and direction of the force. If the force is applied at a fixed point, one would need to solve also the related problem of a bending moment applied on the sphere. In that case, the solution can in principle be obtained from a superposition of the present problem and that associated with a bending moment.

Following the convention of contact mechanics, we take the parabola $x^2/2R$ as an approximation of the surface profile of the cylinder within the contact region (Johnson, 1985). The continuity of displacements across the contact interface leads to

$$\bar{\mathbf{u}} = \begin{bmatrix} \bar{u}_x \\ \bar{u}_y \end{bmatrix} = \begin{bmatrix} \delta_x \\ \delta_y - \frac{x^2}{2R} \end{bmatrix}, \quad (-b < x < a)$$

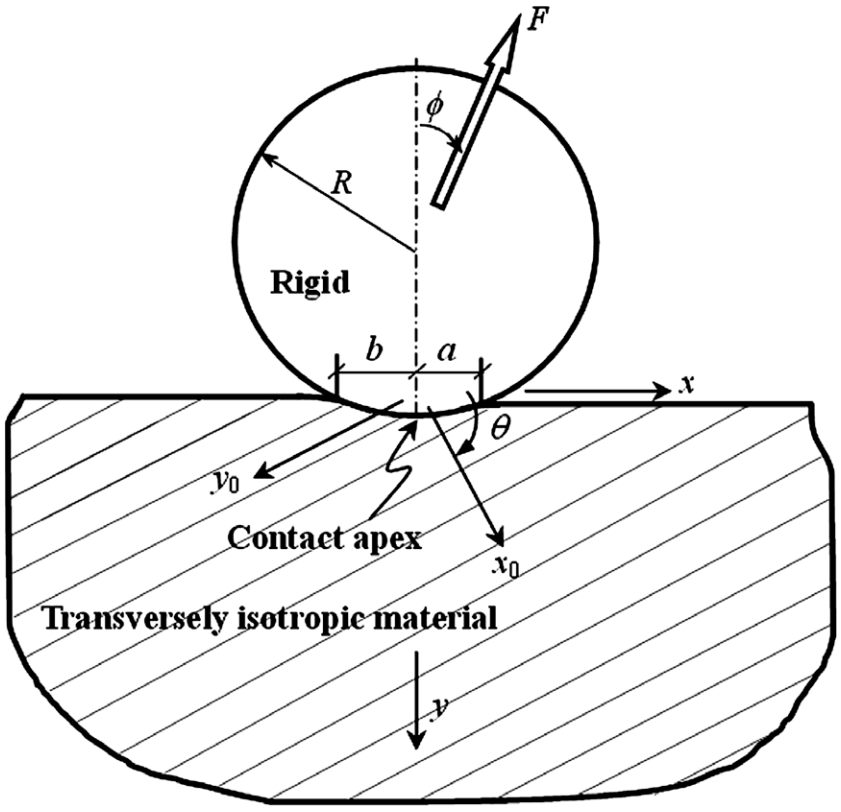

Fig. 1. A rigid cylinder of radius R in non-slipping contact with a transversely isotropic elastic half-space with its symmetry axis inclined at angle θ with respect to the normal of the surface. Cartesian coordinate systems (x_0,y_0) and (x,y) refer to the material coordinates and fixed coordinates, respectively. An external pulling force F is applied on the cylinder at an angle ϕ with respect to the y-axis.

where $\bar{u}_x$, $\bar{u}_y$ stand for the surface displacements of the elastic material, and δ_x, δ_y are translations of the rigid cylinder.

It should be pointed out that the above boundary condition is based on an assumption that, within the contact region, the displacement $\bar{u}_x$ at a point is negligible before contact is established. Rigorously, for a point within the contact area ($-b < x < a$), the displacement $\bar{u}_x$ should consist of two parts. One part corresponds to the deformation before that point enters into contact and another is the subsequent displacement after the contact is established. Because the points within the contact area do not come into contact with the rigid cylinder at the same time, $\bar{u}_x$ is strictly not uniform throughout the contact area. A full account of this effect, however, would severely complicate the analysis (Gladwell, 1980). In this paper, we neglect the pre-contact part of $\bar{u}_x$. A more sophisticated model to fully resolve this issue is left to future work.

The derivative of the surface displacements $\bar{\mathbf{u}}$ with respect to x is given by

$$\mathbf{C} = \frac{\partial \bar{\mathbf{u}}}{\partial x} = \begin{bmatrix} 0 \\ -\frac{x}{R} \end{bmatrix}.$$

Denoting the tractions acting on the surface of the anisotropic material within the contact region by

$$\mathbf{f}(x) = [\,Q(x) \quad P(x)\,]^{\mathrm{T}},$$

the Green's function of an anisotropic elastic half-space (Fan and Keer, 1994; Ting, 1996) correlates the tractions $\mathbf{f}(x)$ and the displacement gradient along the surface through

$$\frac{1}{\pi}\int_{-b}^{a} \frac{\mathbf{L}^{-1}}{s-x}\mathbf{f}(s)ds + \mathbf{S}\mathbf{L}^{-1}\mathbf{f}(x) = \mathbf{C}, \tag{4}$$

where $\mathbf{S}$, $\mathbf{L}$ are the Barnett–Lothe matrices with respect to the fixed coordinates x–y (Fig. 1). Eq. (1) gives the Barnett–Lothe matrices in the material coordinates x_0–y_0, based on which $\mathbf{S}$ and $\mathbf{L}$ can be calculated through following transformations

$$\mathbf{S} = \boldsymbol{\Omega}\mathbf{S}_0\boldsymbol{\Omega}^{\mathrm{T}}, \quad \mathbf{L} = \boldsymbol{\Omega}\mathbf{L}_0\boldsymbol{\Omega}^{\mathrm{T}},$$

where

$$\boldsymbol{\Omega} = \begin{bmatrix} \cos\theta & -\sin\theta \\ \sin\theta & \cos\theta \end{bmatrix}$$

is the transformation matrix from coordinate system (x_0,y_0) to (x,y). Multiplying $\mathbf{L}$ on both sides of Eq. (4) gives rise to

$$\frac{1}{\pi}\int_{-b}^{a} \frac{\mathbf{I}}{s-x}\mathbf{f}(s)ds + \mathbf{B}\mathbf{f}(x) = \mathbf{G}, \tag{5}$$

where

$$\mathbf{I} = \begin{bmatrix} 1 & 0 \\ 0 & 1 \end{bmatrix}, \quad \mathbf{B} = \mathbf{L}\mathbf{S}\mathbf{L}^{-1} = \frac{s_{21}}{L_{11}}\begin{bmatrix} 1/D_{12}^* & -1/D_{11}^* \\ 1/D_{22}^* & -1/D_{21}^* \end{bmatrix}, \quad \mathbf{G} = \mathbf{L}\mathbf{C},$$

with

$$D_{11}^* = \frac{1}{L_{11}\cos^2\theta + L_{22}\sin^2\theta},$$
$$D_{22}^* = \frac{1}{L_{11}\sin^2\theta + L_{22}\cos^2\theta},$$
$$D_{12}^* = D_{21}^* = \frac{1}{(L_{11}-L_{22})\cos\theta\sin\theta}.$$

Following the approach by Chen and Gao (2006), Eq. (5) can be solved. The final solution to the interfacial tractions is given by

$$\begin{bmatrix} Q(x) \\ P(x) \end{bmatrix} = \begin{bmatrix} 2Re\{T_1^+ - T_1^-\} \\ -2D_{11}^* Im\{\bar{d}_1(T_1^+ - T_1^-)\} \end{bmatrix}, \tag{6}$$

where

$$T_1^+ = \frac{xd_1}{4R(1-\eta)} + (b+x)^{-\bar{r}}(a-x)^{-r} \times \left[\frac{d_1}{4\pi \mathrm{i} R(1-\eta)}\int_{-b}^{a}\frac{t(b+t)^{\bar{r}}(a-t)^{r}}{t-x}dt - \kappa_1 \mathrm{i} e^{\pi\varepsilon}\right], \tag{7}$$

$$T_1^- = \frac{xd_1}{4R(1+\eta)} - (b+x)^{-\bar{r}}(a-x)^{-r}e^{-2\pi\varepsilon} \times \left[\frac{d_1}{4\pi \mathrm{i} R(1-\eta)}\int_{-b}^{a}\frac{t(b+t)^{\bar{r}}(a-t)^{r}}{t-x}dt - \kappa_1 \mathrm{i} e^{\pi\varepsilon}\right], \tag{8}$$

and

$$r = \frac{1}{2} + \mathrm{i}\varepsilon, \quad \bar{r} = \frac{1}{2} - \mathrm{i}\varepsilon, \quad \varepsilon = \frac{1}{2\pi}\ln\frac{1+\eta}{1-\eta}, \quad \mathrm{i} = \sqrt{-1},$$
$$\eta = \left|\frac{s_{21}}{L_{11}}\sqrt{D_{22}^{*-1}D_{11}^{*-1} - (D_{12}^{*-1})^2}\right|, \quad d_1 = \frac{\mathrm{i}}{D_{12}^*} + \sqrt{D_{11}^{*-1}D_{22}^{*-1} - D_{12}^{*-2}}.$$

In Eqs. (7) and (8), the constant κ_1 remains to be determined. This can be done by using boundary conditions

$$\int_{-b}^{a} Q(x)dx = F\sin\phi, \quad \int_{-b}^{a} P(x)dx = -F\cos\phi, \tag{9}$$

which gives (see Appendix A)

$$\kappa_1 = -\frac{F(D_{12}^*\cos\phi + D_{11}^*\sin\phi)}{4\pi D_{11}^* D_{12}^*\sqrt{1/D_{11}^* D_{22}^* - 1/D_{12}^{*2}}} + \mathrm{i}\frac{F\sin\phi}{4\pi}.$$

Substituting κ_1 back into Eqs. (7) and (8) yields

$$T_1^+ - T_1^- = 2\cosh(\pi\varepsilon)\frac{1}{\sqrt{(b+x)(a-x)}}\left(\frac{b+x}{a-x}\right)^{\mathrm{i}\varepsilon} \times \left\{-\frac{d_1\mathrm{i}}{4R}\left[\frac{(a+b)^2}{8}(1+4\varepsilon^2) - x\left(x - \frac{a-b}{2}\right)\right] + \frac{F}{4\pi}g(\phi) + \frac{d_1}{4R}(a+b)\varepsilon x,\right\} \tag{10}$$

where

$$g(\phi) = \sin\phi + \frac{\mathrm{i}(D_{12}^*\cos\phi + D_{11}^*\sin\phi)}{D_{11}^* D_{12}^*\sqrt{1/D_{11}^* D_{22}^* - 1/D_{12}^{*2}}}.$$

Eqs. (6) and (10) give the tractions within the contact region. The stress intensity factors can be immediately calculated as follows.

Consider the right contact edge at $x = a$. The stress intensity factors is given by (Wu, 1990; Hwu, 1993; Ting, 1996)

$$\boldsymbol{K}^R = \begin{Bmatrix} K_{\mathrm{II}}^R \\ -K_{\mathrm{I}}^R \end{Bmatrix} = \lim_{x\to a}\sqrt{2\pi}(a-x)^{1/2}\begin{bmatrix} m_{11} & m_{12} \\ m_{21} & m_{22} \end{bmatrix}\begin{Bmatrix} Q(x) \\ P(x) \end{Bmatrix} \tag{11}$$

where

$$m_{11} = \mathrm{Re}\left\{\left[1 + \left(\sqrt{\frac{d_{22}}{d_{11}}} - \sqrt{\frac{d_{11}}{d_{22}}}\right)\mathrm{i}\sin\theta\cos\theta\right]\left(\frac{a-x}{l}\right)^{\mathrm{i}\varepsilon}\right\},$$
$$m_{12} = \left(\frac{\cos^2\theta\sqrt{d_{22}}}{\sqrt{d_{11}}} + \frac{\sin^2\theta\sqrt{d_{11}}}{\sqrt{d_{22}}}\right)\mathrm{Im}\left\{\left(\frac{a-x}{l}\right)^{\mathrm{i}\varepsilon}\right\},$$
$$m_{21} = -\left(\frac{\cos^2\theta\sqrt{d_{11}}}{\sqrt{d_{22}}} + \frac{\sin^2\theta\sqrt{d_{22}}}{\sqrt{d_{11}}}\right)\mathrm{Im}\left\{\left(\frac{a-x}{l}\right)^{\mathrm{i}\varepsilon}\right\},$$
$$m_{22} = \mathrm{Re}\left\{\left[1 - \left(\sqrt{\frac{d_{22}}{d_{11}}} - \sqrt{\frac{d_{11}}{d_{22}}}\right)\mathrm{i}\sin\theta\cos\theta\right]\left(\frac{a-x}{l}\right)^{\mathrm{i}\varepsilon}\right\}.$$

Substituting the tractions into Eq. (11), we have

$$K_{\mathrm{II}}^{R}=\sqrt{2\pi}A\cosh(\pi\varepsilon)(a+b)^{3/2}\mathrm{Re}\{I_1^R\}+\sqrt{2/\pi}(a+b)^{-1/2}A\cosh(\pi\varepsilon)F\mathrm{Re}\{I_2^R\}. \tag{12}$$

$$K_{\mathrm{I}}^{R}=-\sqrt{2\pi}\cosh(\pi\varepsilon)(a+b)^{3/2}[(B\mathrm{Im}\{I_1^R\}+C\mathrm{Re}\{I_1^R\})] -\sqrt{\frac{2}{\pi(a+b)}}\cosh(\pi\varepsilon)F(B\mathrm{Im}\{I_2^R\}+C\mathrm{Re}\{I_2^R\}). \tag{13}$$

where

$$A=\frac{D_{22}^*}{D_{12}^*}\sqrt{\frac{D_{12}^{*2}}{D_{11}^*D_{22}^*}-1}\left(\frac{\cos^2\theta\sqrt{d_{11}}}{\sqrt{d_{22}}}+\frac{\sin^2\theta\sqrt{d_{22}}}{\sqrt{d_{11}}}\right),$$

$$B=\left(\frac{D_{11}^*D_{22}^*}{D_{12}^{*2}}-1\right)\left(\frac{\cos^2\theta\sqrt{d_{11}}}{\sqrt{d_{22}}}+\frac{\sin^2\theta\sqrt{d_{22}}}{\sqrt{d_{11}}}\right),$$

$$C=\frac{D_{11}^*D_{22}^*}{D_{12}^{*2}}\sqrt{\frac{D_{12}^{*2}}{D_{11}^*D_{22}^*}-1}\left(\frac{\cos^2\theta\sqrt{d_{11}}}{\sqrt{d_{22}}}+\frac{\sin^2\theta\sqrt{d_{22}}}{\sqrt{d_{11}}}\right),$$

$$I_1^R=-\frac{d_1}{4R}\left(\frac{a+b}{l}\right)^{\mathrm{i}\varepsilon}\left[\left(\frac{1}{2}(1+4\varepsilon^2)-\frac{2a}{(a+b)}\right)\mathrm{i}-\frac{4a}{(a+b)}\varepsilon\right],$$

$$I_2^R=\left(\frac{a+b}{l}\right)^{\mathrm{i}\varepsilon}g(\phi).$$

Thus the corresponding energy release rate is given by (Wu, 1990; Hwu, 1993)

$$G^{\mathrm{R}}=\frac{1}{4}(\mathbf{K}^R)^{\mathrm{T}}\mathbf{E}\mathbf{K}^R, \tag{14}$$

where the matrix $\mathbf{E}$ is (Appendix B)

$$\mathbf{E}=\frac{1}{\cosh^2(\pi\varepsilon)}\mathbf{L}^{-1}. \tag{15}$$

Upon the substitution of Eqs. 12, 13, 15 into (14), the energy release rate for the right contact edge is given by

$$G^R=\frac{D_{22}^*D_{12}^{*2}B^2}{D_{12}^{*2}-D_{11}^*D_{22}^*}\left[\frac{(a+b)^3}{2}\pi|I_1^R|^2+\frac{F^2}{2\pi(a+b)}|I_2^R|^2+(a+b)F\mathrm{Re}\{\bar{I}_1^RI_2^R\}\right], \tag{16}$$

where $\bar{I}_1^R$ stands for the complex conjugate of I_1^R.

Likewise, the stress intensity factors and energy release rate at the left contact edge ($x=-b$) can be obtained as

$$K_{\mathrm{II}}^{\mathrm{L}}=-\sqrt{2\pi}A\cosh(\pi\varepsilon)(a+b)^{3/2}\mathrm{Re}\{I_1\} +\sqrt{2/\pi}(a+b)^{-1/2}A\cosh(\pi\varepsilon)F\mathrm{Re}\{I_2\} \tag{17}$$

$$K_{\mathrm{I}}^{\mathrm{L}}=-\sqrt{2\pi}\cosh(\pi\varepsilon)(a+b)^{3/2}[(B\mathrm{Im}\{I_1^{\mathrm{L}}\}+C\mathrm{Re}\{I_1^{\mathrm{L}}\})] -\sqrt{\frac{2}{\pi(a+b)}}\cosh(\pi\varepsilon)F(B\mathrm{Im}\{I_2^{\mathrm{L}}\}+C\mathrm{Re}\{I_2^{\mathrm{L}}\}) \tag{18}$$

$$G^{\mathrm{L}}=\frac{D_{22}^*D_{12}^{*2}B^2}{D_{12}^{*2}-D_{11}^*D_{22}^*}\left[\frac{(a+b)^3}{2}\pi|I_1^{\mathrm{L}}|^2+\frac{F^2}{2\pi(a+b)}|I_2^{\mathrm{L}}|^2. +(a+b)F\mathrm{Re}\{\bar{I}_1^{\mathrm{L}}I_2^{\mathrm{L}}\}\right], \tag{19}$$

where

$$I_1^{\mathrm{L}}=-\frac{d_1}{4R}\left(\frac{a+b}{l}\right)^{-\mathrm{i}\varepsilon}\left[\left(\frac{1}{2}(1+4\varepsilon^2)-\frac{2b}{(a+b)}\right)\mathrm{i}+\frac{4b}{(a+b)}\varepsilon\right],$$

$$I_2^{\mathrm{L}}=\left(\frac{a+b}{l}\right)^{-\mathrm{i}\varepsilon}g(\phi).$$

At equilibrium, the energy release rates at both sides should be equal to the surface energy w_{ad} (Johnson, 1985), implying

$$\left(\frac{F}{w_{ad}}\right)^2\frac{|g(\phi)|^2}{2\pi}+\frac{1}{4}\frac{F}{w_{ad}}\left(\frac{a+b}{R}\right)^2\left(\frac{R}{D_{11}^*w_{ad}}\right) \times\mathrm{Re}\left\{D_{11}^*\bar{d}_1g(\phi)\left[\left(\frac{1}{2}(1+4\varepsilon^2)-\frac{2a}{(a+b)}\right)\mathrm{i}+\frac{4a}{(a+b)}\varepsilon\right]\right\} +\frac{\pi}{32}\left(\frac{a+b}{R}\right)^4\left(\frac{R}{D_{11}^*w_{ad}}\right)^2\frac{D_{11}^*}{D_{22}^*}\left|\left(\frac{1}{2}(1+4\varepsilon^2)-\frac{2a}{(a+b)}\right)\mathrm{i} -\frac{4a}{(a+b)}\varepsilon\right|^2-\frac{a+b}{R}\frac{R}{D_{11}^*w_{ad}}\frac{D_{11}^*(D_{12}^{*2}-D_{11}^*D_{22}^*)}{D_{22}^*D_{12}^{*2}B^2}=0 \tag{20}$$

and

$$\left(\frac{F}{w_{ad}}\right)^2\frac{|g(\phi)|^2}{2\pi}+\frac{1}{4}\frac{F}{w_{ad}}\left(\frac{a+b}{R}\right)^2\left(\frac{R}{D_{11}^*w_{ad}}\right) \times\mathrm{Re}\left\{D_{11}^*\bar{d}_1g(\phi)\left[\left(\frac{1}{2}(1+4\varepsilon^2)-\frac{2b}{(a+b)}\right)\mathrm{i}-\frac{4b}{(a+b)}\varepsilon\right]\right\} +\frac{\pi}{32}\left(\frac{a+b}{R}\right)^4\left(\frac{R}{D_{11}^*w_{ad}}\right)^2\frac{D_{11}^*}{D_{22}^*}\left|\left(\frac{1}{2}(1+4\varepsilon^2)-\frac{2b}{(a+b)}\right)\mathrm{i} +\frac{4b}{(a+b)}\varepsilon\right|^2-\frac{a+b}{R}\frac{R}{D_{11}^*w_{ad}}\frac{D_{11}^*(D_{12}^{*2}-D_{11}^*D_{22}^*)}{D_{22}^*D_{12}^{*2}B^2}=0 \tag{21}$$

Considering

$$\sqrt{\frac{D_{11}^*}{D_{22}^*}-(\frac{D_{11}^*}{D_{12}^*})^2}=\frac{\sqrt{L_{11}L_{22}}}{L_{11}\cos^2\theta+L_{22}\sin^2\theta}=\frac{\sqrt{L_{22}/L_{11}}}{\cos^2\theta+L_{22}/L_{11}\sin^2\theta},$$

$$\frac{D_{11}^*}{D_{22}^*}=\frac{\sin^2\theta+L_{22}/L_{11}\cos^2\theta}{\cos^2\theta+L_{22}/L_{11}\sin^2\theta},$$

$$\frac{D_{11}^*}{D_{12}^*}=\frac{(1-L_{22}/L_{11})\sin\theta\cos\theta}{\cos^2\theta+L_{22}/L_{11}\sin^2\theta},$$

$$\frac{D_{11}^*D_{22}^*}{D_{12}^{*2}}=\frac{(L_{22}/L_{11}-1)^2\sin^2\theta\cos^2\theta}{(\cos^2\theta+L_{22}/L_{11}\sin^2\theta)(\sin^2\theta+L_{22}/L_{11}\cos^2\theta)},$$

Eqs. (20) and (21) actually correlate the normalized adhesion force F/w_{ad} and the normalized contact width $(a+b)/R$ in an implicit manner. Given L_{22}/L_{11}, $R/(D_{11}^*w_{ad})$, η, θ and ϕ, the evolution of F/w_{ad} with $(a+b)/R$ can be numerically calculated.

4. Numerical solution

Taking $L_{22}/L_{11}=100$, $R/(D_{11}^*w_{ad})=100$, $\eta=0.2$, $\theta=30^\circ$, the variation of the contact width with the contact force is shown in Fig. 2 where different pulling angles are considered, including $\phi=0^\circ$, 30°, 60°, 90°. Clearly, the evolution of contact width with the applied load depends on the pulling angle. The pull-off force, or the force required to pull the cylinder away from the anisotropic solid, exhibits strong direction-dependence. Among the four pulling angles under consideration, the pull-off force for $\phi=30^\circ$ stands out for its substantially higher magnitude. In addition, one can notice that all curves, instead of extending to infinitely, terminate at a certain compressive load. At first glance, this observation may seem unphysical because of the intuition that any contact size can be achieved as long as the two solids are compressed hard enough. In reality, such limitation on the achievable contact width results from the non-slipping assumption we have adopted. To illustrate this point, we can just simply consider the isotropic case with material properties $ER/2(1-\nu^2)w_{ad}=100$, $\nu=0.375$, where E is the Young's modulus, ν is the Poisson's ratio and w_{ad} is the surface energy. For non-slipping contact, the above model can be used directly by taking $L_{22}/L_{11}=1$, $\theta=0^\circ$, $\eta=0.2$, $R/(D_{11}^*w_{ad})=100$. Assuming that the load is applied in the vertical direction (i.e. $\phi=0^\circ$), the variation of contact width as a function of the contact force is shown in Fig. 3, along with the corresponding solution for frictionless contact (Chaudhury et al., 1996). It can be seen that the two models agree very well in the tensile regime ($F>0$).

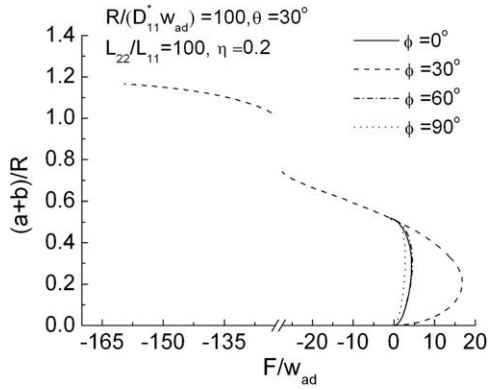

Fig. 2. Variation of the normalized contact width $(a+b)/R$ as a function of the normalized pulling force F/w_{ad} for different pulling angles $\phi = 0°, 30°, 60°, 90°$. Here $\theta = 30°$, $\eta = 0.2$, $L_{22}/L_{11} = 100$, $R/(D^*_{11}w_{ad}) = 100$.

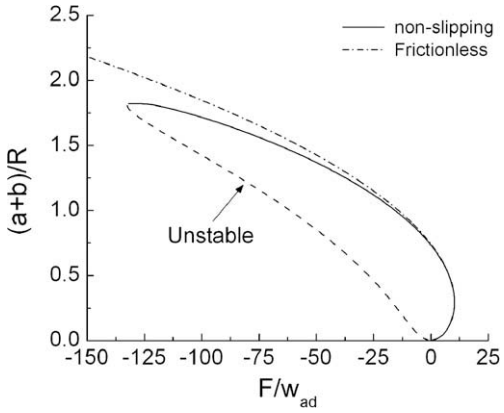

Fig. 3. Comparison of the contact width as a function of the pulling force in the case of non-slipping contact with an isotropic solid and the corresponding result in the case of frictionless contact. The material is assumed isotropic with $\frac{ER}{2(1-\nu^2)w_{ad}} = 100$, $\nu = 0.375$ and the pulling angle is taken as $\phi = 0°$.

However, in the compressive regime ($F < 0$), they give distinct predictions of the contact width. While the frictionless model predicts that the contact width will increase monotonically with increasing compressive force, the non-slipping contact model shows a looped force-contact width relationship. According to the derivative of the energy release rate with respect to the contact width, we find that the equilibrium states defined by the lower branch of this loop are unstable. For this reason, we did not show the unstable branches of the curves in Fig. 2. These results show that stable non-slipping contact can be achieved only at limited compressive load. As the compressive load is increased beyond a critical value, the non-slipping condition can not be ensured and slipping at the contact edges would occur, resulting in a new contact configuration similar to the "stick-slip" process. Further discussions in this aspect are beyond the scope of the current model.

The ratio of a/b for the stable solutions in Fig. 2 is shown in Fig. 4. It can be seen that a/b varies within a narrow range of 0.99–1.12 when the load is applied along the symmetry axis of the transversely isotropic material (i.e., $\phi = \theta = 30°$), suggesting that the contact region can be roughly treated as symmetric with respect to the contact apex ($x = 0$). In contrast, if the pulling angle deviates from the symmetry axis, the contact region could become significantly asymmetric depending on the magnitude of the load. These observations show that the contact zone symmetry assumed in the previous work of Chen and Gao (2007) is approximately valid only when pulled along the symmetry axis of the transversely isotropic solid.

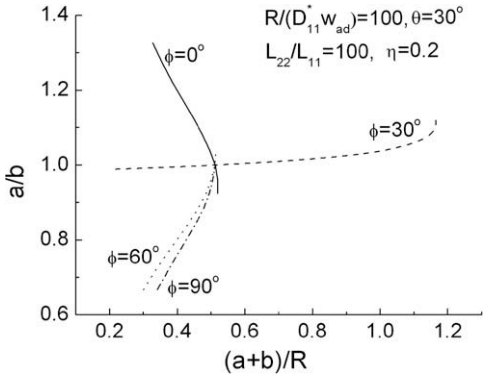

Fig. 4. Variation of the symmetry ratio a/b as a function of the contact width for the stable solutions shown in Fig. 2. This ratio was assumed to be 1 in the study of Chen and Gao (2007).

In order to understand the effect of anisotropy on non-slipping adhesion, we have considered additional cases with different degrees of anisotropy such as $L_{22}/L_{11} = 1$, 10, 100, 1000. Given $\eta = 0.2$, $R/(D^*_{11}w_{ad}) = 100$, Fig. 5 shows variation of the normalized pull-off force $(F/F_0)_{\text{pull-off}}$ as a function of the pulling angle ϕ for materials with various tilting angles θ and degrees of anisotropy. Here $(F_0)_{\text{pull-off}}$ stands for the pull-off force at $\phi = 0°$. It can be seen that for the "quasi-isotropic" cases ($L_{22}/L_{11} = 1$), the pull-off force does not strongly depend on the pulling angle. With the increase of L_{22}/L_{11}, the pull-off force becomes more and more direction-dependent. While the maximum pull-off force occurs at the stiffest direction $\phi = \theta$, the minimum takes place in the most compliant direction $\phi = \theta - \pi/2$ $(0 \leqslant \theta \leqslant \pi/2)$. The difference between the maximum and minimum depends on the anisotropy of the material. The higher the anisotropy, the more significant the difference.

Fig. 6 shows the normalized critical contact width $[(a+b)/(a+b)_0]_{\text{pull-off}}$ as a function of the pulling angle ϕ, where $[(a+b)_0]_{\text{pull-off}}$ denotes the critical contact width for $\phi = 0°$. Except for the case of $\theta = 90°$ (Fig. 6d), the contact width exhibits a minimum value near the stiffest direction $\phi = \theta$. If we define the *adhesion strength* as

$$\sigma = \frac{F_{\text{pull-off}}}{(a+b)_{\text{pull-off}}},$$

where $F_{\text{pull-off}}$ and $(a+b)_{\text{pull-off}}$ are the adhesion force and contact width at pull-off, the variation of the normalized adhesion strength with the pulling angle is shown in Fig. 7. One can see that the adhesion strength is almost direction-independent in all "quasi-isotropic" cases, whereas it exhibits strong directional dependence in the anisotropic cases. Similarly, the maximum adhesion strength is always achieved at $\phi = \theta$, while the minimum takes place around $\phi = \theta - \pi/2$.

5. Discussion and summary

In this paper, we revisited the non-slipping adhesive contact problem of Chen and Gao (2007) between a rigid cylinder and an anisotropic (transversely isotropic) medium subjected to an inclined pulling force. An implicit assumption in Chen and Gao (2007) is that the contact region remains symmetric with respect to the center of the cylinder. Here we have removed this assumption and derived the correct solution to the non-slipping contact problem defined by Chen and Gao (2007). In the compressive regime ($F < 0$), our solution shows that the non-slipping contact may not be possible if the load level is too high. Under this circumstance, slipping between the two surfaces may occur. In the tensile regime ($F > 0$), it is found that the pull-off force between the cylin-

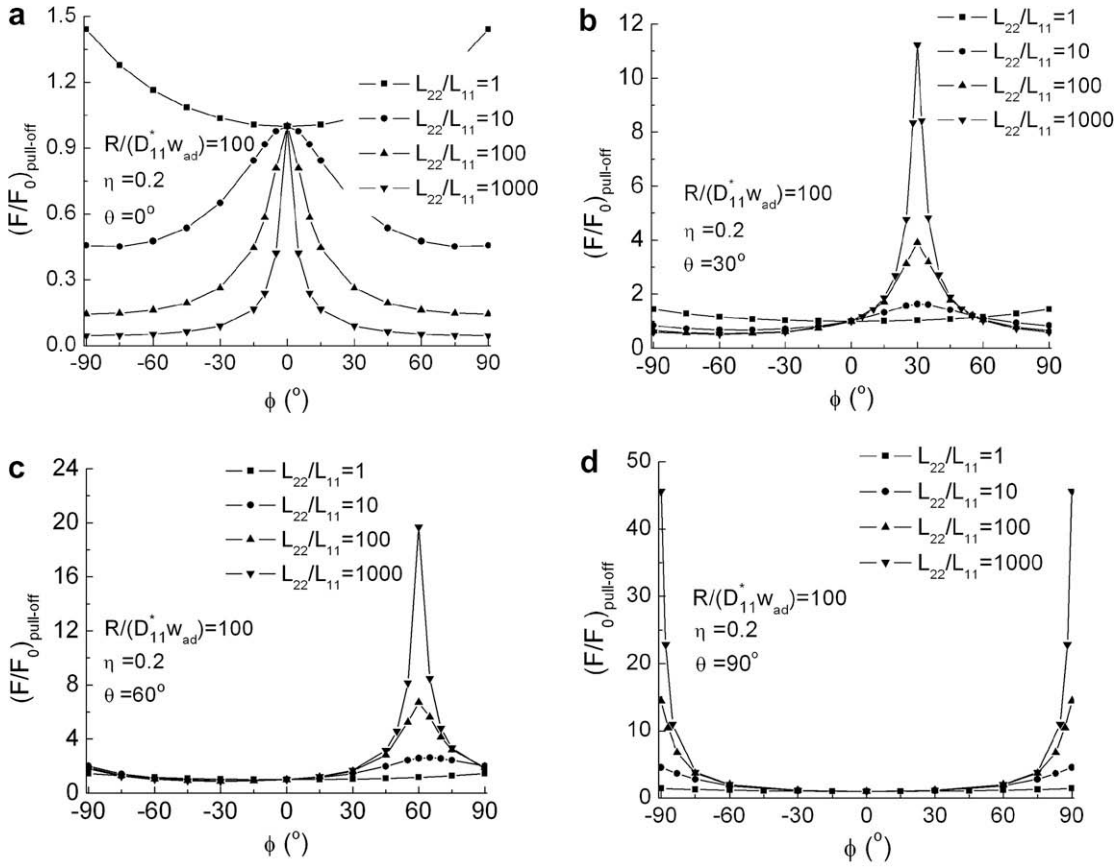

Fig. 5. The normalized pull-off force $(F/F_0)_{\text{pull-off}}$ as a function of the pulling angle ϕ for $\eta = 0.2$, $R/(D^*_{11}w_{ad}) = 100$, L_{22}/L_{11} = 1,10,100,1000 with tilting angle θ equal to (a) 0°, (b) 30°, (c) 60°, (d) 90°, respectively.

der and substrate depends on the direction of pulling. Adhesion is strongest in the stiff direction and weakest in the compliant direction. Similar phenomenon has been previously reported in the cracked interface model and summarized as a "stiff-adhere and soft release" principle (Yao and Gao, 2006). The difference between strong and weak adhesion depends on the degree of anisotropy of the medium. The stronger the anisotropy, the greater the difference. Therefore, materials with strong anisotropy can be designed to achieve orientation-dependent adhesion in reversible adhesion devices (Yao and Gao, 2006). Qualitatively similar conclusions were drawn by Chen and Gao (2007), despite the additional constraint of symmetric contact region.

Recently, experimental studies on directional adhesion have been conducted. For example, Yao et al. (2008) measured the adhesion force between a spherical probe and a film-terminated tilted fiber sample made of PDMS. As expected, the measured adhesion force exhibits directional dependence. But no peak detachment force has been observed in the longitudinal direction of the fibers as predicted by the theoretical model. The cause of this discrepancy between theory and experiment is still under investigation and might in part be attributed to the dependence of critical energy release rate on the mode mixity of stress at the contact edges. In our theoretical model, we have assumed that the critical energy release rate remains a constant, equal to the surface energy w_{ad}. In reality, it may depend on the mode mixty of stress at the contact edges (Jensen et al., 1990). Another possibility might be the finite thickness of the experimental sample, in contrast to the half-space assumption in the theoretical model. Moreover, our theoretical analysis was carried out within the framework of small-deformation elasticity, in which the orientation of anisotropy axis remains fixed during loading. In the experiments, the compliant PDMS fibers tend to experience large deformation, resulting in large rotation of the anisotropy axis. More sophisticated models are needed to capture the details of the experiments.

Appendix A

Details of how constant κ_1 is determined by the boundary conditions of Eq. (9) are as follows.

From Eqs. (7) and (8), we have

$$T_1^+ - T_1^- = \frac{x d_1 \eta}{2R(1-\eta^2)} - \mathrm{i}(1+e^{-2\pi\varepsilon})(b+x)^{-\bar{r}}(a-x)^{-r} \times \left[\frac{d_1}{4\pi R(1-\eta)}\int_{-b}^{a}\frac{t(b+t)^{\bar{r}}(a-t)^{r}}{t-x}dt + \kappa_1 e^{\pi\varepsilon}\right] \tag{A1}$$

Let us first focus our attention on the integral on the right-hand side of Eq. (1).

$$\begin{aligned}\int_{-b}^{a}\frac{t(b+t)^{\bar{r}}(a-t)^{r}}{t-x}dt &= \int_{-b}^{a}(b+t)^{\bar{r}}(a-t)^{r}dt + x\int_{-b}^{a}\frac{(b+t)^{\bar{r}}(a-t)^{r}}{t-x}dt \\ &= \frac{(a+b)^2}{8}(1+4\varepsilon^2)\pi\,\mathrm{sech}(\pi\varepsilon) \\ &\quad + x\frac{(a+b)}{2}\int_{-1}^{1}\frac{(1+t)^{\bar{r}}(1-t)^{r}}{t-\left(\frac{2x}{a+b}-\frac{a-b}{a+b}\right)}dt\end{aligned} \tag{A2}$$

Defining $x' = \frac{2x}{a+b} - \frac{a-b}{a+b}$, Eq. (A2) can be rewritten as

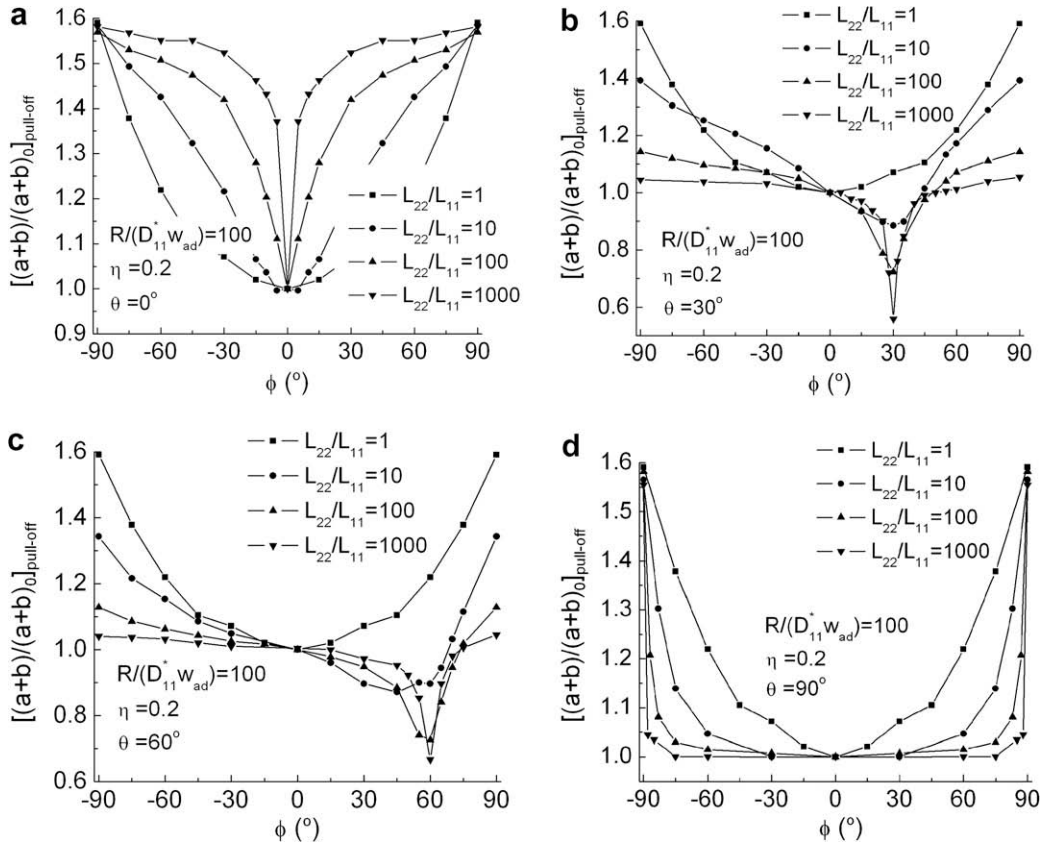

Fig. 6. The normalized contact width $[(a+b)/(a+b)_0]_{\text{pull-off}}$ as a function of the pulling angle ϕ for $\eta = 0.2$, $R/(D_{11}^{*}w_{ad}) = 100$, L_{22}/L_{11} = 1,10,100,1000 with tilting angle θ equal to (a) 0°, (b) 30°, (c) 60°, (d) 90°, respectively.

$$\int_{-b}^{a}\frac{t(b+t)^{\bar{r}}(a-t)^{r}}{t-x}dt=\frac{(a+b)^{2}}{8}(1+4\varepsilon^{2})\pi\sec h(\pi\varepsilon)+\frac{(a+b)x}{2}\int_{-1}^{1}\frac{(1+t)^{\bar{r}}(1-t)^{r}}{t-x'}dt, \tag{A3}$$

In Eq. (A3), the integrand is singular at $t = x'$. The Cauchy principal value of this integral can be calculated as follows.

Define a complex function

$$\widetilde{F}(z)=\frac{1}{2\pi i}\int_{-1}^{1}\frac{(1+t)^{\bar{r}}(1-t)^{r}}{t-z}dt. \tag{A4}$$

Given complex variable $z(z\notin[-1,1])$, substitution of variable leads to

$$\begin{aligned}\widetilde{F}(z)&=\frac{1}{2\pi i}\int_{-1}^{1}\frac{(1+t)^{\bar{r}}(1-t)^{r}}{t-z}dt\\&=\frac{1}{2\pi i}\int_{0}^{\pi}\frac{\sin^{2}\theta}{\cos\theta-z}\left(\frac{1-\cos\theta}{1+\cos\theta}\right)^{i\varepsilon}d\theta\\&=-\frac{1}{2\pi i}\pi\sec h(\pi\varepsilon)[-2i\varepsilon+z-ie^{-\pi\varepsilon}(1-z)^{r}(1+z)^{\bar{r}}].\end{aligned} \tag{A5}$$

For a real variable $x' \in [-1,1]$,

$$\widetilde{F}^{+}(x')=-\frac{1}{2\pi i}\pi\sec h(\pi\varepsilon)[-2i\varepsilon+x'-ie^{-\pi\varepsilon}(1-x')^{r}(1+x')^{\bar{r}}], \tag{A6}$$

$$\widetilde{F}^{-}(x')=-\frac{1}{2\pi i}\pi\sec h(\pi\varepsilon)[-2i\varepsilon+x'+ie^{\pi\varepsilon}(1-x')^{r}(1+x')^{\bar{r}}], \tag{A7}$$

where $\widetilde{F}^{+}(x')=\lim_{y\to0^{+}}\widetilde{F}(x'+yi)$ and $\widetilde{F}^{-}(x')=\lim_{y\to0^{-}}\widetilde{F}(x'+yi)$. On the other hand, according to the Plemelj formulae (Carrier et al., 1983), we have

$$\widetilde{F}^{+}(x')-\widetilde{F}^{-}(x')=(1-x')^{r}(1+x')^{\bar{r}}, \tag{A8}$$

$$\widetilde{F}^{+}(x')+\widetilde{F}^{-}(x')=\frac{1}{\pi i}(\text{P.V.})\int_{-1}^{1}\frac{(1+t)^{\bar{r}}(1-t)^{r}}{t-x'}dt \tag{A9}$$

Substituting Eqs. (A6) and (A7) into (A9) leads to

$$(\text{P.V.})\int_{-1}^{1}\frac{(1+t)^{\bar{r}}(1-t)^{r}}{t-x'}dt=(2i\varepsilon-x')\pi\sec h(\pi\varepsilon)-\pi i(1-x')^{r}(1+x')^{\bar{r}}\tanh(\pi\varepsilon). \tag{A10}$$

Inserting Eq. (A10) into Eq. (A3) yields

$$\begin{aligned}\int_{-b}^{a}\frac{t(b+t)^{\bar{r}}(a-t)^{r}}{t-x}dt=\pi\sec h(\pi\varepsilon)&\left[\frac{(a+b)^{2}}{8}(1+4\varepsilon^{2})\right.\\&\left.+i(a+b)\varepsilon x-x\left(x-\frac{a-b}{2}\right)\right]\\&-\frac{a+b}{2}x\pi i(1-x')^{r}(1+x')^{\bar{r}}\tanh(\pi\varepsilon)\end{aligned} \tag{A11}$$

Combining Eqs. (A11) and (A1) gives rise to

$$\begin{aligned}T_{1}^{+}-T_{1}^{-}=2i\cosh(\pi\varepsilon)(b+x)^{-\bar{r}}(a-x)^{-r}&\left\{-\frac{d_{1}}{4R}\left[\frac{(a+b)^{2}}{8}(1+4\varepsilon^{2})\right.\right.\\&\left.\left.+i(a+b)\varepsilon x-x^{2}+\frac{a-b}{2}x\right]-\kappa_{1}\right\}\end{aligned} \tag{A12}$$

where the relations $\frac{1+\eta}{1-\eta}=e^{2\pi\varepsilon}$, $e^{2\pi ri}=-e^{-2\pi\varepsilon}$ and $e^{-\pi ri}=-ie^{\pi\varepsilon}$ have been used. Therefore,

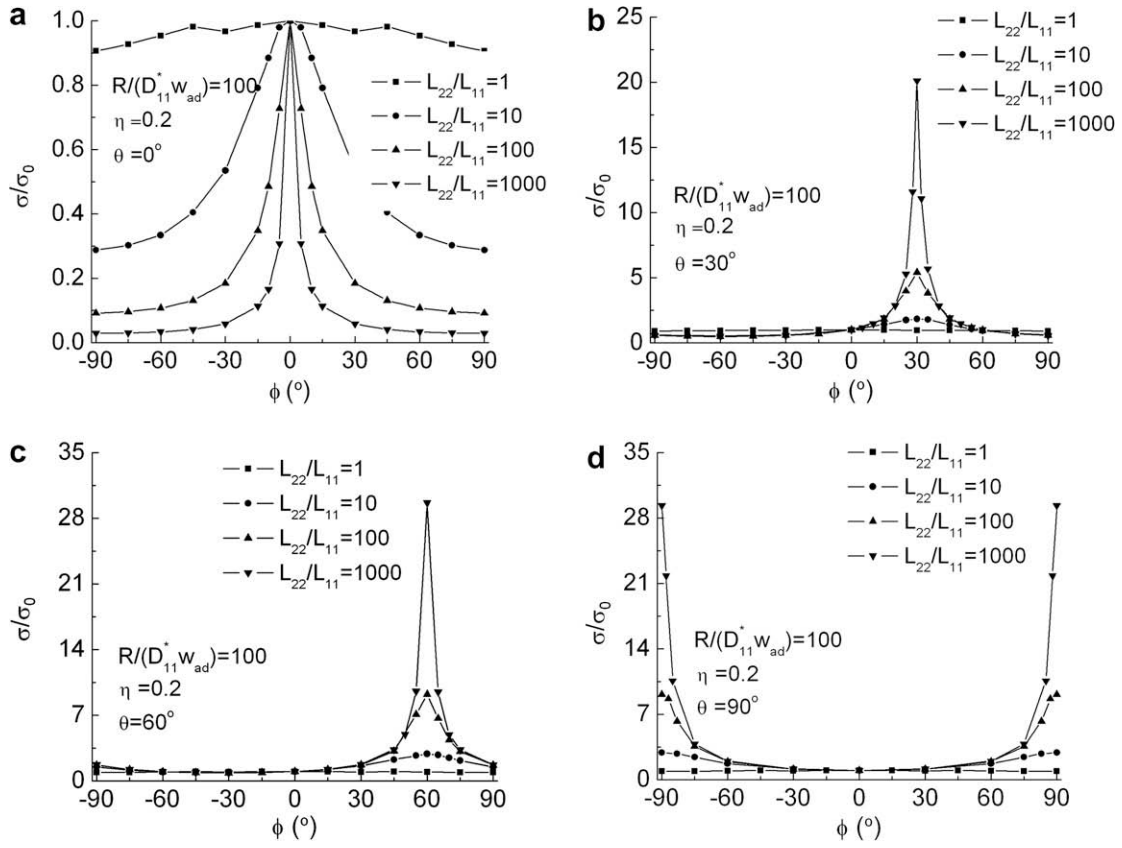

Fig. 7. The normalized adhesion strength σ/σ_0 as a function of the pulling angle ϕ for $\eta = 0.2$, $R/(D^*_{11}w_{ad}) = 100$, L_{22}/L_{11} = 1,10,100,1000 with tilting angle θ equal to (a) 0°, (b) 30°, (c) 60°, (d) 90°, respectively.

$$\int_{-b}^{a}(T_1^+ - T_1^-)dx = 2\mathrm{i}\cosh(\pi\varepsilon)\left\{-\left[\frac{(a+b)^2 d_1}{32R}(1+4\varepsilon^2)+\kappa_1\right]I_a - \frac{d_1}{4R}\left[\mathrm{i}(a+b)\varepsilon+\frac{a-b}{2}\right]I_b+\frac{d_1}{4R}I_c\right\}, \tag{A13}$$

with

$$I_a = \int_{-b}^{a}(b+x)^{-\bar{r}}(a-x)^{-r}dx = \pi\,\mathrm{sech}(\pi\varepsilon), \tag{A14}$$

$$I_b = \int_{-b}^{a}x(b+x)^{-\bar{r}}(a-x)^{-r}dx = \pi\,\mathrm{sech}(\pi\varepsilon)[\mathrm{i}(a+b)\varepsilon+\frac{a-b}{2}], \tag{A15}$$

$$I_c = \int_{-b}^{a}x^2(b+x)^{-\bar{r}}(a-x)^{-r}dx = \pi\,\mathrm{sech}(\pi\varepsilon)\left[\frac{(a+b)^2}{8}(1-4\varepsilon^2)+(a^2-b^2)\mathrm{i}\varepsilon+\left(\frac{a-b}{2}\right)^2\right] \tag{A16}$$

Inserting Eqs. A14, A15, and A16 into Eq. (A13), we have

$$\int_{-b}^{a}(T_1^+ - T_1^-)dx = -2\mathrm{i}\pi\kappa_1. \tag{A17}$$

Substituting Eq. (6) into the boundary conditions of Eq. (9) and then taking advantage of Eq. (A17) yield the real and imaginary parts of κ_1 as

$$\mathrm{Re}\{\kappa_1\} = -\frac{F(D^*_{12}\cos\phi + D^*_{11}\sin\phi)}{4\pi D^*_{11}D^*_{12}\sqrt{1/D^*_{11}D^*_{22}-1/D^{*2}_{12}}}, \quad \mathrm{Im}\{\kappa_1\} = \frac{F\sin\phi}{4\pi}, \tag{A18}$$

which gives

$$\kappa_1 = -\frac{F(D^*_{12}\cos\phi + D^*_{11}\sin\phi)}{4\pi D^*_{11}D^*_{12}\sqrt{1/D^*_{11}D^*_{22}-1/D^{*2}_{12}}} + \mathrm{i}\frac{F\sin\phi}{4\pi}. \tag{A19}$$

Appendix B

Following its definition (Wu, 1990; Hwu, 1993), **E** can be expressed in terms of Barnett–Lothe tensors as

$$\mathbf{E} = \mathbf{L}^{-1} + (\mathbf{SL}^{-1})\mathbf{L}(\mathbf{SL}^{-1}) = (1+s_{12}s_{21})\mathbf{L}^{-1}. \tag{B1}$$

Eqs. (2)–(4) implies

$$\frac{s_{12}}{L_{11}} = -\frac{s_{21}}{L_{22}}. \tag{B2}$$

Eq. (B1) therefore can be rewritten as

$$\mathbf{E} = \left(1-\frac{L_{22}}{L_{11}}s_{21}^2\right)\mathbf{L}^{-1} = (1-\eta^2)\mathbf{L}^{-1}. \tag{B3}$$

Considering $\varepsilon = \frac{1}{2\pi}\ln\frac{1+\eta}{1-\eta}$, Eq. (B3) can be simplified further to be

$$\mathbf{E} = \frac{1}{\cosh^2(\pi\varepsilon)}\mathbf{L}^{-1}. \tag{B4}$$

References

Arzt, E., Gorb, S., Spolenak, R., 2003. From micro to nano contacts in biological attachment devices. Proc. Natl. Acad. Sci. USA 100, 10603–10606.
Autumn, K., Liang, Y.C., Hsieh, S.T., Zesch, W., Chan, W.P., Kenny, T.W., Fearing, R., Full, R.J., 2000. Adhesion forces of a single gecko foot-hair. Nature 405, 681–685.
Carrier, G.F., Krook, M., Pearson, C.E., 1983. Functions of a Complex Variable: Theory and Technique. Hod Books, Ithaca, NY.
Chaudhury, M.K., Weaver, T., Hui, C.Y., Kramer, E.J., 1996. Adhesive contact of cylindrical lens and a flat sheet. J. App. Phys. 80, 30–37.
Chen, S., Gao, H., 2006. Non-slipping adhesive contact of an elastic cylinder on stretched substrates. Proc. R. Soc. Lond. A 462, 211–228.
Chen, S., Gao, H., 2007. Bio-inspired mechanics of reversible adhesion: orientation-dependent adhesion strength for non-slipping adhesive contact with transversely isotropic elastic materials. J. Mech. Phys. Solids 55, 1001–1015.

Dongye, C., Ting, T.C.T., 1989. Explicit expression of Barnett–Lothe tensors and their associated tensors for orthotropic materials. Q. Appl. Math. 47, 723–734.
Fan, H., Keer, L.M., 1994. Two-dimensional contact on anisotropic elastic half-space. J. Appl. Mech. 61, 250–255.
Gao, H., Yao, H., 2004. Shape insensitive optimal adhesion of nanoscale fibrillar structure. Proc. Natl. Acad. Sci. USA 101, 7851–7856.
Gao, H., Wang, X., Yao, H., Gorb, S., Artz, E., 2005. Mechanics of hierarchical adhesion structures of gecko. Mech. Mater. 37, 275–285.
Gladwell, G.M.L., 1980. Contact problems in the classical theory of elasticity. Sijthoff and Noordhoff, Alphen aan den Rijn, The Netherlands.
Hwu, C., 1993. Fracture parameters for the orthotropic bimaterial interface cracks. Eng. Fract. Mech. 45, 89–97.
Jensen, H., Hutchinson, J., Kim, K.-S., 1990. Decohesion of a cut prestressed film on a substrate. Int. J. Solids Struct. 26, 1099–1114.
Johnson, K.L., 1985. Contact Mechanics. Cambridge University Press, Cambridge.
Ting, T.C.T., 1996. Anisotropic Elasticity. Oxford University Press, New York.
Wu, K.C., 1990. Stress intensity factors and energy release rate for interfacial cracks between dissimilar anisotropic materials. J. Appl. Mech. 57, 882–886.
Yao, H., Gao, H., 2006. Bio-inspired mechanics of robust and releasable adhesion on rough surface. J. Mech. Phys. Solids 54, 1120–1146.
Yao, H., Della Rocca, G., Guduru, P.R., Gao, H., 2008. Adhesion and sliding response of a biologically inspired fibrillar surface: experimental observations. J.R. Soc. Interface 5, 723–733.